

RESEARCH ARTICLE

Exon- and contraction-dependent functions of titin in sarcomere assembly

Yu-Huan Shih^{1,*}, Alexey V. Dvornikov¹, Ping Zhu¹, Xiao Ma^{1,2}, Maengjo Kim¹, Yonghe Ding¹ and Xiaolei Xu^{1,†}

ABSTRACT

Titin-truncating variants (TTNts) are the major cause of dilated cardiomyopathy (DCM); however, allelic heterogeneity (TTNts in different exons) results in variable phenotypes, and remains a major hurdle for disease diagnosis and therapy. Here, we generated a panel of *ttn* mutants in zebrafish. Four single deletion mutants in *ttn.2* or *ttn.1* resulted in four phenotypes and three double *ttn.2/ttn.1* mutants exhibited more severe phenotypes in somites. Protein analysis identified *ttn^{xu071}* as a near-null mutant and the other six mutants as hypomorphic alleles. Studies of *ttn^{xu071}* uncovered a function of titin in guiding the assembly of nascent myofibrils from premyofibrils. By contrast, sarcomeres were assembled in the hypomorphic *ttn* mutants but either became susceptible to biomechanical stresses such as contraction or degenerated during development. Further genetic studies indicated that the exon usage hypothesis, but not the toxic peptide or the Cronos hypothesis, could account for these exon-dependent effects. In conclusion, we modeled TTNtv allelic heterogeneity during development and paved the way for future studies to decipher allelic heterogeneity in adult DCM.

KEY WORDS: Sarcomere assembly, TALEN, Titin, Zebrafish, Allelic heterogeneity

INTRODUCTION

The gene that encodes the largest protein, titin (*TTN*) (Labeit et al., 1992), was recently established as a causative gene for cardiomyopathies and muscular dystrophies (LeWinter and Granzier, 2013; Chauveau et al., 2014). Approximately 25% of patients with end-stage dilated cardiomyopathy (DCM) have truncating mutations in *TTN* (Herman et al., 2012). However, the clinical translation of this genetic knowledge has been complicated (Norton et al., 2013). While *TTN*-truncating variants (TTNts) in exons encoding A-band domains cause DCM, many TTNts in exons encoding Z-disk domains are benign (Herman et al., 2012). Moreover, mutations found in patients with limb-girdle muscular dystrophy type 2J and tibial muscular dystrophy are more common in C-terminal exons that encode M-line domains of *TTN* (Hackman et al., 2002; Udd et al., 2005). A dominant toxic peptide hypothesis has been proposed to explain the allelic heterogeneity phenotypes, whereby A-band, but not Z-disk, truncated *TTN* is incorporated into normal sarcomeres to exert toxic effects on heart function (Herman

et al., 2012). On the other hand, exon-dependent phenotypes could be explained by the differential use of the 363 exons of the human *TTN* gene (reviewed by Guo et al., 2010). In line with this loss-of-function hypothesis, a study of patients with DCM identified a correlation between exon usage and severity of the DCM phenotype (Roberts et al., 2015). More recently, the identification of a short *TTN* isoform, termed Cronos, prompted a new hypothesis. Driven by an internal promoter located in the intron before exon 240 of *TTN*, the Cronos isoform only encodes A-band and M-line domains and misses all Z-disk and most I-band domains (Zou et al., 2015). As such, the authors posited that mutations in A-band exons are deleterious because of the disrupted Cronos isoform, whereas mutations in Z-disk exons are benign because of the normal Cronos isoform.

One *TTN* molecule spans half of a sarcomere, and sequences of *TTN* domains from N-terminus to C-terminus match the different sarcomeric substructures – including the Z-disk, I-band, A-band and M-line (Labeit and Kolmerer, 1995). Therefore, full-length *TTN* has been proposed to act as a template during *de novo* sarcomere assembly (Trinick, 1996). Moreover, the A-band region of *TTN* has been proposed to function as a ‘molecular ruler’ to govern the assembly of thick filaments and define the length of the A-band at 1.6 μm (Whiting et al., 1989). Despite multiple genetic studies of *TTN* in the past 20 years, however, the template and ruler hypotheses remain inconclusive. Several *Ttn* mutants have been generated in mice, including a TTNtv affecting the A-band (Gramlich et al., 2009) and internal deletion mutants that remove the N2B exon (Radke et al., 2007) or an M-line exon (Weinert et al., 2006). However, all mutants were not null, which contributes to the inconclusive findings regarding function of *TTN* in *de novo* sarcomere assembly.

Zebrafish is a new vertebrate model for studying sarcomere assembly (Schoenebeck and Yelon, 2007; Huang et al., 2009; Sanger et al., 2009; Yang et al., 2014b). From a large-scale screen using N-ethyl-N-nitrosourea as a mutagen, a group of *ttn* mutants, named *pickwick* (*pik*), have been identified (Xu et al., 2002). Because of the gigantic gene size, the precise location of the mutation was only mapped for the *pik^{m171}* allele. Other zebrafish *ttn* mutant alleles, such as *runzel* (Steffen et al., 2007) and *herzschlag* (Myhre et al., 2014), were reported later, but the precise locations of these mutations were not identified. Zebrafish have two *ttn* homologs, *ttna* and *ttnb* (Seeley et al., 2007), which are referred to here as *ttn.2* and *ttn.1*, respectively, according to a new nomenclature (Table S1). We previously used splice-blocking morpholinos to target the N2B and N2A exons of *ttn.2* and *ttn.1* (Seeley et al., 2007). However, concerns about the specificity of the morpholino technology (Kok et al., 2015; Rossi et al., 2015) and the advent of gene-editing technologies such as transcription activator-like effector nuclease (TALEN)-based methods (Campbell et al., 2013) prompted the generation of stable *ttn* knockout zebrafish mutants. Whereas a panel of *ttn.2* mutants have previously been generated using CRISPR-Cas9 technology (Zou et al., 2015), here,

¹Department of Biochemistry and Molecular Biology, Division of Cardiovascular Diseases, Mayo Clinic, 200 First St SW, Rochester, MN 55905, USA. ²Mayo Graduate School, Mayo Clinic College of Medicine, Rochester, MN 55905, USA. ^{*}Present address: Department of Molecular, Cell, and Cancer Biology, University of Massachusetts Medical School, Worcester, MA 01605, USA.

[†]Author for correspondence (xu.xiaolei@mayo.edu)

 X.X., 0000-0002-4928-3422

we used TALEN (transcription activator-like effector nuclease) technology to introduce a series of deletion mutations. We detected five phenotypes of different severity from seven different *ttn* mutants, recapitulating exon-dependent phenotypes. We characterized a near-null *ttn* mutant and provided the first genetic evidence uncovering functions of titin in *de novo* sarcomere assembly.

RESULTS

Deletional mutations in four different exons of zebrafish *ttn.2* or *ttn.1* result in four distinct phenotypes

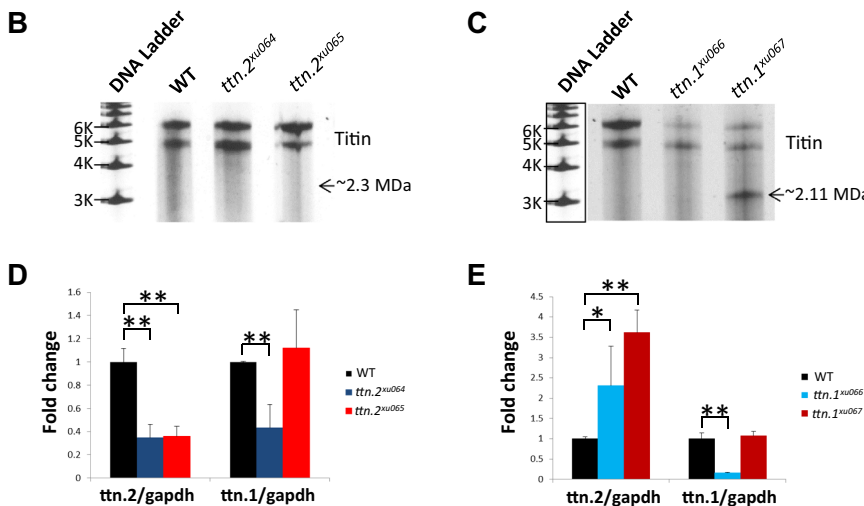
We designed TALEN pairs targeting sequences in exons 5 and 201 of *ttn.2*, which encode domains in the Z-disk and the A-band, respectively (*xu064* and *xu065*; Fig. 1A), and in exons 5 and 165 of *ttn.1*, which encode the corresponding domains in the Z-disk and the A-band (*xu066* and *xu067*; Fig. 1A). For each TALEN, at least two deletion mutant alleles with two different frameshifts were obtained (data not shown). Because the two alleles exhibited the same phenotypes, suggesting no off-target effects, we focused on one allele for each mutant locus.

To determine the protein level of titin in these mutants, we used vertical agarose gels followed by silver staining (Warren et al., 2003) and detected two Ttn bands in larvae at 2 days post-fertilization (dpf). Surprisingly, all four mutants showed the same two bands as in wild-type (WT) larvae (Fig. 1B,C). No truncated Ttn bands of smaller size were detected in the *ttn.2* mutants (Fig. 1B), which might be partially ascribed to nonsense-mediated mRNA decay since *ttn.2* mRNA expression was decreased by more than half in both *ttn.2* mutants (Fig. 1D). We detected a shorter Ttn band at ≈ 2.11 MDa in *ttn.1^{xu067}* (Fig. 1C). The *ttn.1* transcript was decreased in *ttn.1^{xu066}* but remained unchanged in the *ttn.1^{xu067}* mutant (Fig. 1E). At the mRNA level, *ttn.2* and *ttn.1* seemed to regulate each other, as indicated by the decrease in *ttn.1* mRNA expression in *ttn.2^{xu064}* (Fig. 1D) and the 2- to 3-fold increase in *ttn.2* mRNA expression in both *ttn.1^{xu066}* and *ttn.1^{xu067}* mutants (Fig. 1E).

Both *ttn.2* homozygous mutants showed pericardial edema with reduced ventricle size (Fig. S1A), slightly decreased heart rates (Fig. S1B), and nearly depleted shortening fraction at 2 dpf (Fig. S1C). Their hearts appeared as a string at 5 dpf, the bodies exhibited severe abdominal edema at 7 dpf, and most embryos died



Fig. 1. Four *ttn* deletion mutants are hypomorphic *ttn* alleles. (A) Schematic representation of the *ttn.2* and *ttn.1* mutants. Sequences targeted by TALEN pairs are underlined. Presumed stop codons are shown in red text. Restriction enzyme recognition sites for genotyping purposes are boxed. Amino acids after the shift in reading frame are underlined. (B) Protein extracts from 2 dpf larvae of *ttn.2^{xu064}* and *ttn.2^{xu065}* mutants analyzed by protein gel electrophoresis. A 1 kb DNA ladder is used for molecular size reference. The arrow indicates the anticipated region for the Cronos isoform. WT, wild type. (C) Protein extracts from 2 dpf *ttn.1^{xu066}* and *ttn.1^{xu067}* mutants analyzed by protein gel electrophoresis. The arrow indicates the smaller band with estimated size. (D,E) *ttn.2* and *ttn.1* mRNA expression in *ttn.2^{xu064}* and *ttn.2^{xu065}* larvae (D) and *ttn.1^{xu066}* and *ttn.1^{xu067}* larvae (E) relative to WT, as revealed by qPCR using primers to exons in the M-line. Data shown are the average of four experiments. *gapdh* was used as a reference gene. Means±s.d., N=4. *P<0.05, **P<0.01.



at ~10 dpf (Fig. S1D,E). Compared with *ttn.2^{xu064}* mutants, which still swam at 3 dpf, the *ttn.2^{xu065}* mutants were completely paralyzed (Fig. S1D). Compared with well-assembled myofibrils in somites of WT fish at 2 dpf, myofibrils in *ttn.2^{xu064}* appeared slightly misaligned, with reduced sarcomere length (mean±s.d. length, 1.89±0.23 µm in *ttn.2^{xu064}* versus 2.21±0.16 µm in WT; Fig. 2A); myofibrils in *ttn.2^{xu065}* were severely disrupted, with only residue-riated myofibrils consisting of much shorter sarcomeres (1.32±0.20 µm; Fig. 2A).

Unlike *ttn.2*, the *ttn.1* mutants appeared normal until 5 dpf, when an inflated swim bladder failed to develop (Fig. S1D), and both mutants exhibited decreased mobility upon touch stimulation with a needle. *ttn.1^{xu066}* mutants died at ~12 dpf, whereas *ttn.1^{xu067}* mutants survived up to 17 dpf (Fig. S1E). Consistently, disarranged myofibrils were noted in *ttn.1^{xu066}* somites at 9 dpf when myofibrils in *ttn.1^{xu067}* were normal (Fig. 2B). Together, our data revealed four distinct phenotypes resulting from deletion mutations in four different exons of *ttn.2* or *ttn.1*, recapitulating the allelic heterogeneity of TTNts in DCM (Herman et al., 2012).

Exon-dependent phenotypes of *ttn.2* and *ttn.1* may be explained by the exon usage hypothesis

The observation of more severe sarcomere phenotypes in *ttn.2^{xu065}* than *ttn.2^{xu064}* seems consistent with findings in patients with DCM – that is, a TTNtv in an A-band exon, but not a Z-disk exon, results in DCM (Herman et al., 2012). To directly test the toxic peptide hypothesis, we generated a *ttn.2^{xu068}* cis-compound mutant by introducing a Z-disk nonsense mutation into *ttn.2^{xu065/+}* (Fig. 2C). The *ttn.2^{xu068}* cis-compound homozygous mutant exhibited comparable defects to those in the *ttn.2^{xu065}* mutant, which indicates that introducing a Z-disk nonsense mutation fails to rescue the phenotype (Fig. 2D). Together with the lack of truncated proteins in our vertical agarose gels (Fig. 1B), our data argue against the toxic peptide hypothesis.

To assess the Cronos hypothesis (Zou et al., 2015), we tested for the presence of Cronos by protein gel analysis but detected no bands in the region corresponding to the predicted size for the Cronos protein in either WT embryos or *ttn* mutants (Fig. 1B,C).

To test the exon usage hypothesis (Roberts et al., 2015), we used absolute quantitative reverse transcriptase polymerase chain reaction (qPCR) to compare the expression level of these four exons, with the N2B and N2A exons as controls. In 2 dpf WT larvae, the expression level of exon 5 in *ttn.2* was half that of exon 201 (Fig. 3A) and expression of exon 5 in *ttn.1* was 6-fold higher than that of exon 165 (Fig. 3B). The different expression levels of the two exons in *ttn.2* remain at 5 dpf (Fig. S3B,C) and 9 dpf, respectively (Fig. S3D,E), whereas expression levels of the two exons in *ttn.1* become similar. We posited that the different exon usage might result from alternative splicing events. Using qPCR with primers targeting exon 2 of *ttn.2* and exon 7 of *ttn.1*, we detected alternative splicing events around exon 5 of *ttn.2* but not around exon 5 of *ttn.1* (Fig. 3C). Three alternative splicing isoforms of *ttn.2* were found, all of which skipped exon 5 (Fig. 3D). In contrast, we found no alternative splicing events around exon 199 to exon 203 of *ttn.2* (Fig. S2A,B) but did note exon-skipping events on exon 165 and exon 166 of *ttn.1* (Fig. 3E,F). These findings are consistent with the exon usage data and correlate with the severity of phenotypes in these four *ttn.2* or *ttn.1* mutants.

Double *ttn.2* and *ttn.1* mutants lack compensation and result in more severe phenotypes

The presence of two full-size Ttn bands in all four *ttn* mutants containing a single deletion mutation suggested their identity as hypomorphic mutants. To test this hypothesis, we generated the *ttn^{xu069}* (double-Z) mutant that contains nonsense mutations in Z-disk exons of both *ttn* homologs and the *ttn^{xu070}* (double-A) mutant that contains deletion mutations in A-band exons in both *ttn* homologs (Fig. 4A). The higher Ttn band disappeared in both

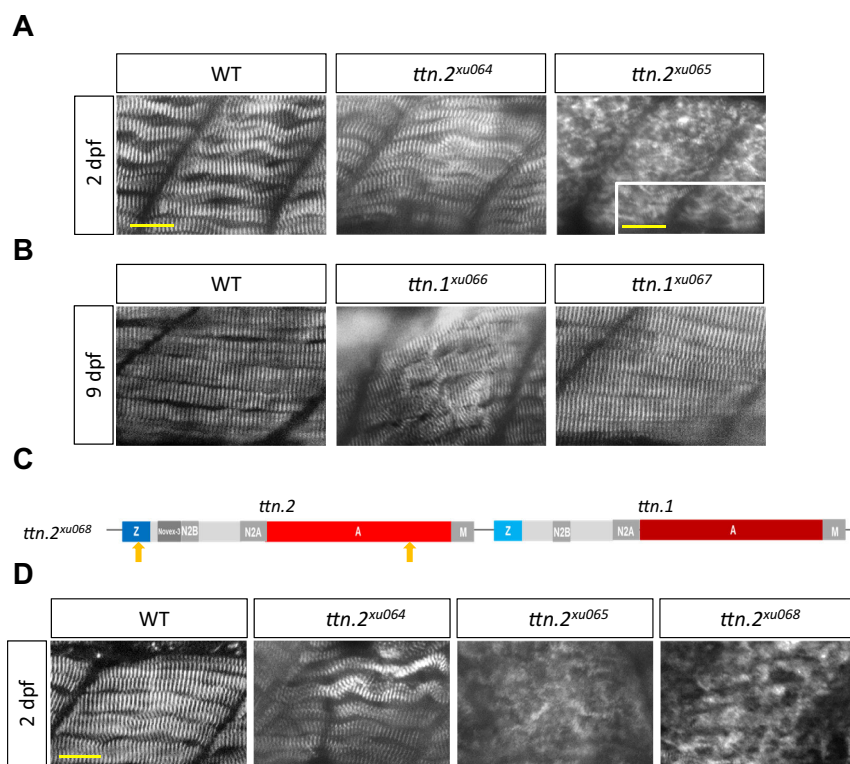


Fig. 2. Exon-dependent functions of titin in sarcomere assembly in somites. (A) *ttn.2^{xu065}*, but not *ttn.2^{xu064}*, exhibits disrupted Z-disk formation in somites at 2 dpf. Shown are whole-mount immunostaining for α -Actinin. The inset is a magnified image showing residual striated structure in *ttn.2^{xu065}*. (B) *ttn.1^{xu066}*, but not *ttn.1^{xu067}*, exhibits sarcomere disarray in somites at 9 dpf. (C) Schematic representation of the *ttn.2* cis double mutant *ttn.2^{xu068}*. Arrows indicate locations of mutations. (D) Immunostaining for α -Actinin in somites at 2 dpf indicates that the Z-disk structure in *ttn.2^{xu065}* and *ttn.2^{xu068}* mutants is disrupted to the same extent. Scale bars: 20 µm and 8 µm (inset in A).

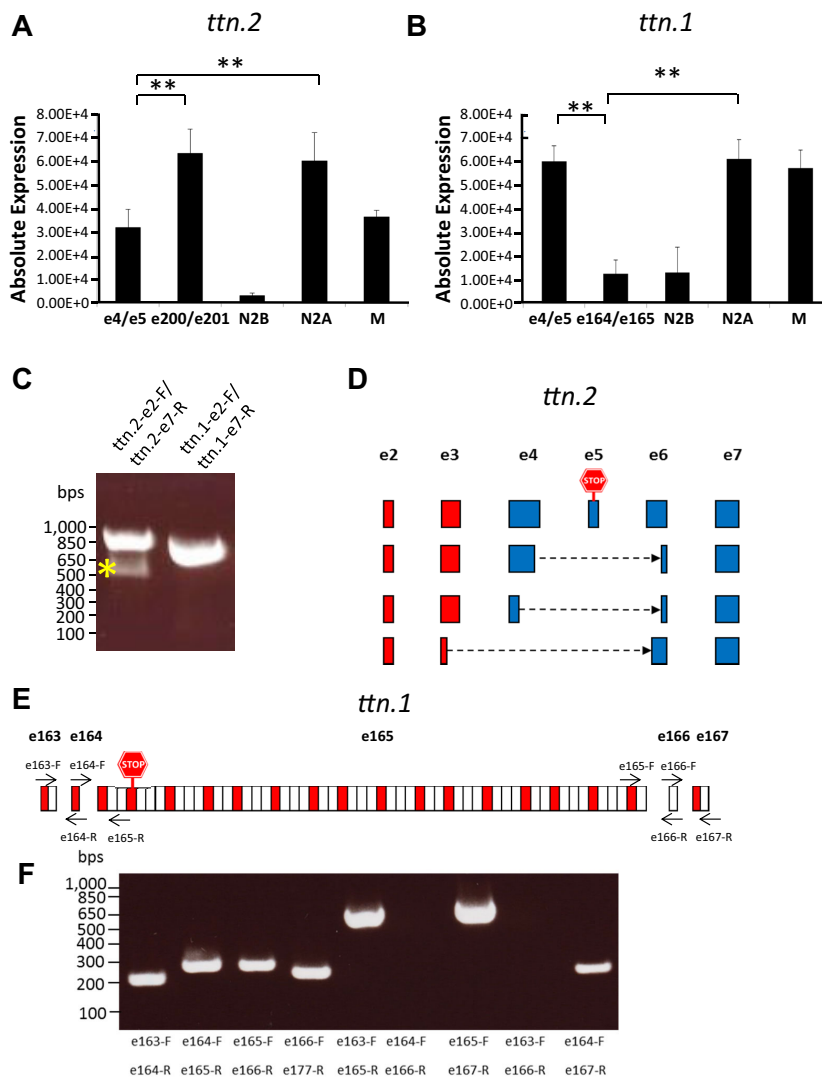


Fig. 3. Alternative splicing and usage of different exons in WT *ttn.2* and *ttn.1*. (A) Exon usage was quantified using absolute qPCR with primers targeting exons of *ttn.2*. (B) Exon usage in *ttn.1*. Means \pm s.d., $N=5$. $^{**}P<0.01$. (C) An alternative splicing event can be detected for exon 5 of *ttn.2* but not *ttn.1*. Smaller PCR products (*) can be detected by PCR using primers targeting exon (e)2 and e7 of *ttn.2*. (D) Schematic representation of three splicing isoforms around e5 of *ttn.2*. (E) Schematic representation of an exon-skipping event around exon 165 of *ttn.1*. The red and white blocks indicate Ig and Fn-III domains, respectively. Premature stop codons introduced by the TALEN mutants are labeled. (F) RT-PCR using different combinations of primers targeting ~e163–e167 of *ttn.1* revealed an exon-skipping event on exon 165 and 166.

double-Z and double-A mutants, but the lower band remained (Fig. 4B,C). The compensation of the Ttn protein level was at least partially removed at the transcriptional level, as indicated by the suppression of *ttn.2* mRNA upregulation induced by *ttn.1* mutations in these double mutants (Fig. 4D). Compared with *ttn.2*^{xu064} and *ttn.1*^{xu067} mutants that could swim, further reduction of Ttn.1 in *ttn.2*^{xu064} or reduction of Ttn.2 in *ttn.1*^{xu067} paralyzed the fish (data not shown). Myofibrils were severely disrupted in both double-Z and double-A mutants (Fig. 4E).

Because the lower Ttn band still existed in these cis double mutants, we targeted two highly used exons of *ttn.2* and *ttn.1*, and generated *ttn*^{xu071} (Fig. 5A). Both Ttn bands were undetectable in *ttn*^{xu071} (Fig. 5B), and both *ttn.2* and *ttn.1* transcripts were reduced (Fig. 5C). Sarcomeres were disrupted to a similar degree as in the double-A and double-Z mutants (Fig. 5D). Only residual thick-filament-like structures can be detected in the electron micrographs (Fig. 5E).

The functional redundancy between *ttn.2* and *ttn.1* was further underscored by our data on *ttn.2*^{xu071/+};*ttn.1*^{xu066}, a mutant generated by crossing *ttn.1*^{xu066} into *ttn*^{xu071/+}. In contrast to the *ttn.2*^{xu065/+} and *ttn.1*^{xu066} mutants with normal striated Z-disks at 2 dpf, *ttn.2*^{xu071/+};*ttn.1*^{xu066} larvae showed myofibril disarray (Fig. 5F).

Characterization of the near-null *ttn*^{xu071} mutant uncovers the functions of Ttn in sarcomere and thick filament assembly

In a zebrafish embryo at the 18-somite stage, different stages of sarcomere assembly in the slow muscle can be observed simultaneously (Sanger et al., 2009). Z-bodies formed dotted structures with a mean regular distance of 0.89 ± 0.19 μ m (mean \pm s.d.) at the 15th somite, became better striated with an expanded sarcomere length of 1.35 ± 0.27 μ m at the 12th somite, and further expanded to 2.14 ± 0.2 μ m at the 6th somite (Fig. 6A,C). At the 6th somite, the Z-bodies completed the initial lateral growth process and formed the wider Z-disk with a width of 0.86 ± 0.18 μ m (Fig. 6A,B). Ttn started to be expressed as random dots at the 18th somite but became striated at the 12th to 13th somites (Fig. S4).

Because *ttn*^{xu071} is the first near-null *ttn* mutant allele in a vertebrate (Fig. S4), we interrogated the functions of *ttn* in *de novo* sarcomere assembly. The earlier steps of Z-body assembly appeared normal in *ttn*^{xu071}, as indicated by a regular dotted pattern of Z-bodies at an average distance of 0.80 ± 0.18 μ m at the 15th somite and the expansion of the striated Z-bodies to 1.18 ± 0.21 μ m at the 12th somite (Fig. 6A,C). However, these Z-bodies failed to grow further in either width (0.45 ± 0.09 μ m; Fig. 6B) or length (1.29 ± 0.16 μ m) at the 6th somite (Fig. 6A,C).

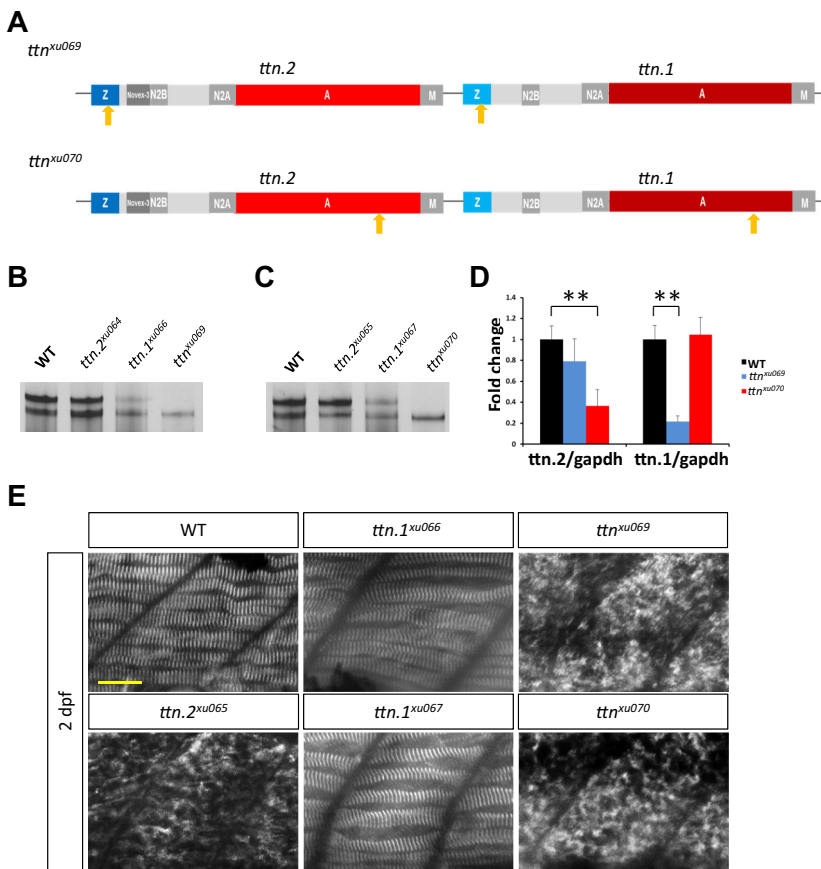


Fig. 4. Mutants *ttn^{xu69}* and *ttn^{xu070}* overcome protein compensation and exhibit more severe phenotypes. (A) Schematic representation of two double mutants, *ttn^{xu069}* and *ttn^{xu070}*. Arrows indicate locations of mutations. (B) Protein extracts from 2 dpf larvae of *ttn^{xu69}* mutants analyzed by 2% SDS-agarose gel and silver staining. (C) Protein analysis of *ttn^{xu070}*. (D) *ttn.2* and *ttn.1* mRNA expression levels in *ttn^{xu070}* and *ttn^{xu69}* mutants, as revealed by qPCR using primers targeting *ttn.2* and *ttn.1*, respectively. Means±s.d., N=5. **P<0.01. (E) Immunostaining of 2 dpf embryos for α-Actinin. Scale bar: 20 μm.

Similarly, the assembly process of the thick filament in the slow muscle can also be revealed in a single embryo at the 18-somite stage using an F59 antibody. We found that myosin filaments in

the WT zebrafish were partially bundled along the long axis of the somite, with an average thick filament length of $0.8 \pm 0.15 \mu\text{m}$ at the 15th somite, became better organized and striated with expanded

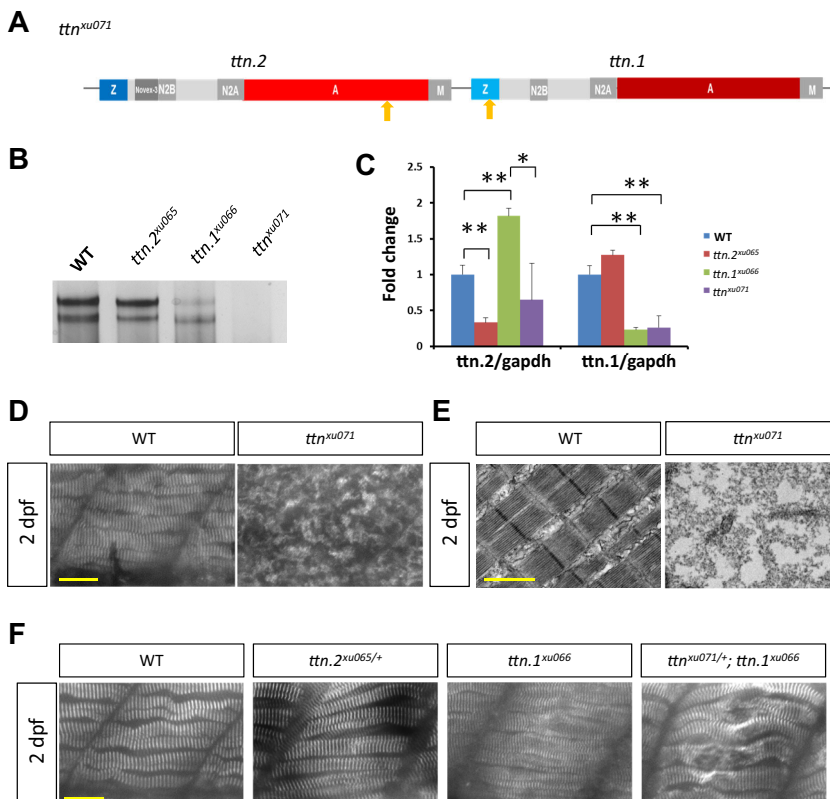


Fig. 5. Generation of a *ttn.2/1* near-null mutant by targeting two highly used exons. (A) Schematic representation of the *ttn^{xu071}* mutant. Arrows indicate locations of mutations. (B) Analysis of protein extracts from 2 dpf WT larvae and *ttn.2^{xu065}*, *ttn.1^{xu066}* and *ttn^{xu071}* mutants. (C) qPCR with primers targeting *ttn.2* and *ttn.1*, respectively. Means±s.d., N=5. *P<0.05, ** P<0.01. (D) The Z-disk structure marked by α-Actinin was disrupted in the *ttn^{xu071}* mutant. (E) Electron micrographs of somites of 2 dpf WT and *ttn^{xu071}* mutant larvae. (F) Z-disk structure was normal in *ttn.2^{xu065/+}* and *ttn.1^{xu066}* at 2 dpf, but sarcomere disarray was noted in *ttn^{xu071/+}* and *ttn.1^{xu066}*. Scale bars: 20 μm (D,F) and 1 μm (E).

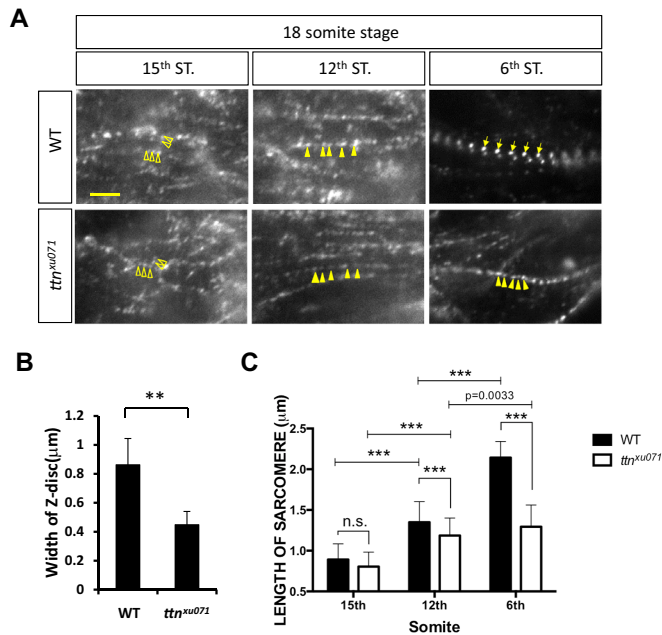


Fig. 6. Phenotypes of *de novo* sarcomere assembly in the *ttn.2/1*-null mutant. (A) WT or *ttn^{xu071}* mutant embryos at the 18-somite stage were stained for α -Actinin. The images were taken at the 6th, 12th and 15th somites (ST). Scale bar: 5 μ m. Z-bodies were scattered as irregular dots (open arrowheads) at the 15th somites and became periodic and aligned longitudinally (solid arrowheads) at the 12th somite. In the 6th somite, Z-bodies underwent lateral growth to form striated Z-disks (arrows) in WT embryos but not in the *ttn^{xu071}* mutant (solid arrowheads). (B) The width of the Z-disc of WT and *ttn^{xu071}* mutants at the 6th somite was quantified. Means \pm s.d. $N=90$ for each group from six embryos. $**P<0.01$. (C) The length of sarcomeres, marked by the distance between two adjacent Z-bodies or Z-disks, in 6th, 12th and 15th somites of WT and *ttn^{xu071}* mutant embryos. The length of sarcomeres did not increase at the 6th somite in the *ttn^{xu071}* mutant compared with WT, where sarcomere length increased to 2.2 μ m. Means \pm s.d. $***P<0.00001$. $N=80$ for each group in different somites from six embryos. n.s., not significant ($P>0.05$).

length (1.46 ± 0.2 μ m) at the 12th somite, and finally formed mature A-bands with a length of 1.64 ± 0.13 μ m at the 6th somite (Fig. 7A,C). Similar results were obtained using an A4.1025 antibody, which also detects myosin heavy chain isoforms (data not shown). Resulting from lateral growth, the width of myosin filaments also expanded to 0.92 ± 0.14 μ m at the 6th somite (Fig. 7B). In contrast, only random myosin dots with a length of 0.83 ± 0.13 μ m could be detected in *ttn^{xu071}* at the 15th somite, which remained unorganized and were 0.87 ± 0.18 μ m long at the 12th somite (Fig. 7A,C). Myosin filaments with a width of 0.6 ± 0.11 μ m and length of 1.1 ± 0.21 μ m did emerge at the 6th somite (Fig. 7A-C). Different from the WT embryos, these thick filaments did not form mature A-bands, which indicates an instructive role for titin in thick filament assembly.

A mutation on exon 5 of *ttn.2* affects sarcomere structure in slow but not fast muscles in a contraction-dependent fashion

In *ttn.2^{xu064}*, sarcomere structures and Z-disks remained relatively normal at 2 dpf (Fig. 2A). Interestingly, thick and thin filaments were undetectable in the middle part of each myofibril, and the blanked middle section was enclosed by two rod-like structures that connected to the remaining myofibrils in each somite segment (Fig. 8A). The rod-like structures could be stained by both Phalloidin and an anti-myosin antibody. This unusual phenotype only occurred in the slow muscles located superficially under the

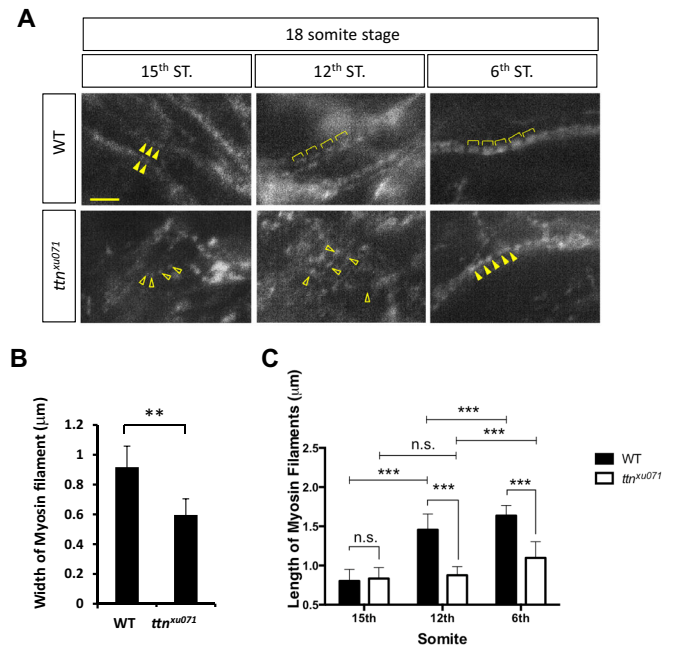


Fig. 7. Phenotypes of thick filament assembly in the *ttn.2/1*-null mutant. (A) Immunostaining was performed in WT or *ttn^{xu071}* mutant embryos at the 18-somite stage with an F59 antibody against the myosin heavy chain. Scale bar: 5 μ m. Myosin filaments were aligned longitudinally (solid arrowheads) at the 15th somite in WT embryos but remain scattered in *ttn^{xu071}* (open arrowheads). Expansion of thick filaments is seen in WT embryos at the 12th and 6th somites (brackets). However, the thick filaments in the *ttn^{xu071}* mutant remain scattered at the 12th somite (open arrowheads) and become aligned at the 6th somite (solid arrowheads). (B) The width of the thick (myosin) filaments of WT and *ttn^{xu071}* mutants at the 6th somite was quantified. Means \pm s.d. $N=84$ for each group from six embryos. $**P<0.01$. (C) The length of myosin filaments in the 6th, 12th and 15th somites of WT and *ttn^{xu071}* mutant embryos. The length of thick filaments does not increase in the *ttn^{xu071}* mutant, whereas thick filament length increases to 1.6 μ m in WT. Means \pm s.d. $***P<0.00001$. $N=80$ for each group in different somites from six embryos. n.s., not significant ($P>0.05$).

skin and not in the fast muscles located deeper and oblique to the anterior-posterior axis (Devoto et al., 1996), as indicated by both Phalloidin staining and immunostaining using antibodies against fast-muscle tropomyosin and myomesin (Fig. 8A,B).

Given that a developing zebrafish larva starts to twitch at 27 hpf, when slow muscle is mainly used (McKeown et al., 2009), we posited that slow-muscle-specific phenotypes in *ttn.2^{xu064}* may be due to the mechanical stress induced by muscle usage in the setting of reduced sarcomere stability. To test this hypothesis, we inhibited muscle contraction by anesthetizing *ttn.2^{xu064}* mutant larvae with 1% tricaine at 24 hpf, right before the first twitch, for 24 h. Indeed, the disrupted myofibrils were significantly rescued (Fig. 8C and Fig. S5). Similar rescuing effects were noted in embryos treated with 10 μ M blebbistatin (data not shown), a myosin inhibitor that inhibits muscle contraction via a different mechanism (Straight et al., 2003). By contrast, the disrupted myofibrils were further exaggerated by increasing muscle contraction via either bleaching the chorion (Zhang et al., 2009) or treatment with galanthamine (Otten and Abdelilah-Seyfried, 2013), an acetylcholine esterase inhibitor (Fig. 8C, Fig. S5, and data not shown). Together, our data suggested that partially decreased expression of Ttn affects the stability of sarcomeres in the slow muscle, resulting in higher susceptibility to damage from mechanical stress. Alternatively, this result might reflect different titin isoform usage in slow and fast muscles.

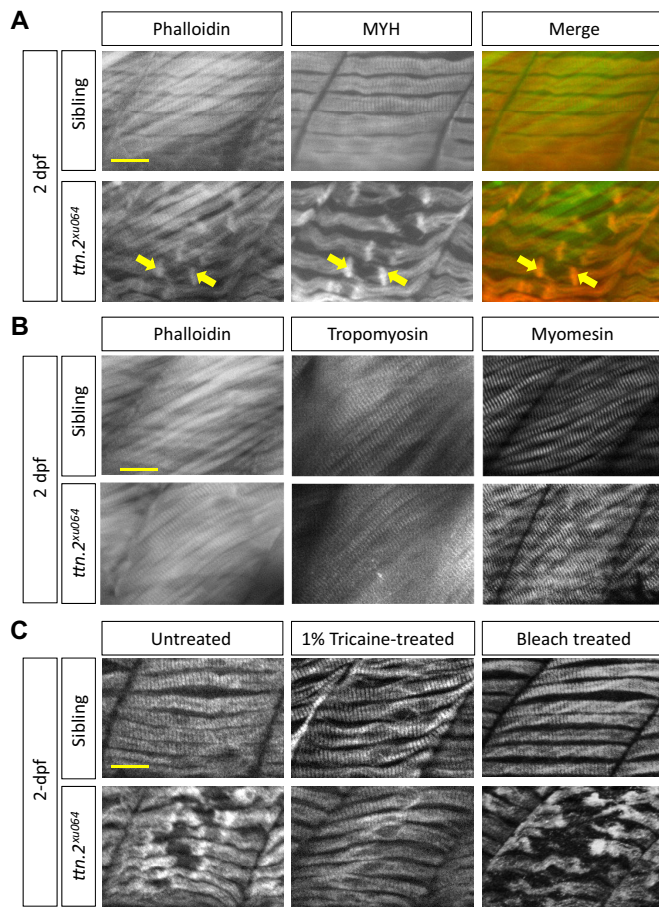


Fig. 8. Contraction-dependent myofibril damage to the slow muscle of *ttn.2^{xu064}*. (A) Slow muscle defects in *ttn.2^{xu064}* embryos. Immunostaining for Myosin and Phalloidin staining to label Actin filaments in 2 dpf embryos. Arrows indicate the two rod-like structures enclosing the damaged myofibril region. (B) Fast muscle is intact in *ttn.2^{xu064}*. Immunostaining with antibodies against Tropomyosin and Myomesin or staining with Phalloidin in 2 dpf embryos. (C) *ttn.2^{xu064}* mutants and siblings treated with 1% tricaine for 24 h or 0.07% bleach at 1 dpf for 5 min were fixed and immunostained for Myosin at 2 dpf. Scale bars: 5 μ m.

DISCUSSION

Generation of hypomorphic and near-null mutants of *ttn* in zebrafish using gene-editing technology

Using TALEN-based genome-editing technology, we generated four zebrafish *ttn* mutants with mutations affecting single exons in either *ttn.2* or *ttn.1* and three double mutants. All mutations were small deletions that purposely shift the reading frame and presumably result in stop codons. However, both Ttn bands could be identified by protein gel analysis of the four single mutants, indicating that they are hypomorphic mutants. No truncated Ttn band was detected in any of the mutants except *ttn.1^{xu067}*. Strong compensational effects must exist, which might include a scavenger system that removes the truncated proteins.

This prediction was validated by our follow-up studies with double mutants. Whereas double-A and double-Z mutants lack the upper band, the *ttn^{xu071}* double mutant lacks both bands, resulting in a near-null mutant. We did not term the mutant as a null because of possible residual Ttn protein that is beyond the detection limit of silver staining. Our data challenge the concept that the upper band represents the product of *ttn.2* and that the lower band denotes the product of *ttn.1* (Steffen et al., 2007). Instead, each Ttn band likely

consists of a mixture of *ttn.2* and *ttn.1* products because neither upper nor lower band can be completely depleted in single mutants. Based on results from mammalian Ttn gels (Granzier and Labeit, 2004), we predict that the two bands might represent N2B- and N2BA-based Ttn isoforms. Given that *ttn.2* consists of 234 exons with a 176,965 bp coding sequence, which is longer than *ttn.1* (201 exons with 137,988 bp coding sequence) (Seeley et al., 2007), our observation further suggests that there is a length-control mechanism for maintaining the size of Ttn proteins.

Our qPCR studies suggest that the length-control mechanisms and the scavenger mechanism might involve regulation at the transcriptional level. We detected significant downregulation of *ttn.2* or *ttn.1* transcripts in all mutants except *ttn.1^{xu067}*, which indicates that nonsense-mediated decay is involved. We detected increased *ttn.2* activation in two *ttn.1* mutants (Fig. 1E), which suggests genetic compensation induced by the loss of *ttn.1*. Of note, the changes at the protein level do not always match the changes at the RNA level, as indicated by the decreased protein bands in *ttn.1^{xu066}* (Fig. 1C), suggesting additional regulation at the translational level. Further detailed studies are warranted using these zebrafish mutants to uncover compensational mechanisms for regulating the length and isoforms of Ttn.

Hypomorphic *ttn* mutants uncover titin functions in maintaining sarcomere integrity

By depleting Ttn proteins to different degrees, we noticed five sarcomeric phenotypes of different severity among the seven *ttn* mutants (Fig. S6). First, *de novo* sarcomere assembly is completely arrested in the double-Z, double-A and near-null mutants (Fig. 4E and Fig. 5D). The phenotypes are indistinguishable among this group using immunostaining assays, despite the fact that Ttn proteins are disrupted to different degrees, ranging from loss of the upper band to loss of both bands. Second, *de novo* sarcomere assembly was also arrested in *ttn.2^{xu065}*, but residue-striated myofibrils could be transiently seen. The *ttn.2^{xu068}* double mutant also belongs to this group. Third, sarcomeres can be successfully assembled in *ttn.2^{xu064}*, despite the disarray of myofibrils shown at 2 dpf. Fourth, sarcomere structure appears normal in *ttn.1^{xu066}* at 2 dpf, but myofibril disarray appears at 9 dpf, and the larvae die at 12 dpf. Fifth, sarcomere assembly appears normal in *ttn.1^{xu067}* at 9 dpf, but the larvae die at 17 dpf.

This panel of different sarcomeric phenotypes clearly demonstrates a crucial function of Ttn in maintaining the integrity of the sarcomere (Fig. S6). A slight decrease in total Ttn protein expression is not sufficient to affect *de novo* sarcomere assembly; however, myofibrils become unstable and exhibit phenotypes under biomechanical stress. It remains to be determined whether the detachment of thin and thick filaments in the center of a myofibril is a common initial subcellular form of damage occurring in patients with a *TTN* mutation.

The generation and characterization of seven *ttn* mutants with defined mutation locations help to interpret other reported zebrafish *ttn* mutants. On the basis of their cardiac phenotypes at 2 dpf, it is reasonable to predict that all *pik* mutants affect *ttn.2* (Xu et al., 2002). By contrast, the late-onset phenotypes in both *ttn.1* mutants are similar to those described in *runzel* (Steffen et al., 2007), which suggests that the *runzel* mutant affects *ttn.1* but not *ttn.2*.

Exon-dependent phenotypes of *ttn* and their underlying mechanisms

As to the mechanism underlying exon-dependent functions of Ttn.2 or Ttn.1 in sarcomere assembly, our data do not favor the toxic

peptide hypothesis for three reasons. First, we did not detect truncated Ttn protein in most *ttn* mutants. Second, although we did detect a truncated Ttn band in the *ttn.I^{xu067}* mutant (but not the *ttn.I^{xu066}* mutant), the phenotype was more severe in the Z-disk *ttn.I^{xu066}* mutant than the A-band *ttn.I^{xu067}* mutant (Fig. 2B). Third, the phenotype of the *ttn.2^{xu068}* cis double mutant was similar to that of *ttn.2^{xu065}* but not *ttn.2^{xu064}* (Fig. 2D).

It remains to be determined whether our conclusions based on fish embryos can be extrapolated to *TTN*-based adult human diseases. Truncated TTN protein was not detected in samples of skeletal muscle (Gerull et al., 2006) or left ventricles (Roberts et al., 2015) from patients with cardiomyopathy. A recent study using engineered induced pluripotent stem cell-derived cardiomyocytes mimicking different A-band truncation mutations from human patients reported a smaller TTN fragment in only one of the three cell lines (Hinson et al., 2015). In contrast, truncated TTN was found in skeletal muscle biopsy specimens from patients with DCM (Gerull et al., 2002) and in a mouse model (Gramlich et al., 2009). Obviously, a much larger sample size is needed to clarify whether truncated Ttn results from TTNts and whether these truncated proteins contribute to pathogenesis.

Our data also do not support the Cronos hypothesis for several reasons: (1) our protein gel analysis failed to detect the Cronos protein, (2) *ttn.I^{xu066}* exhibits more severe phenotypes than *ttn.I^{xu067}* (Fig. 2B) and (3) the double-Z mutant exhibits phenotypes similar to the double-A mutant (Fig. 4E).

Among the three current hypotheses for explaining exon-dependent phenotypes of *ttn.2/1* mutants, our data agree only with the exon usage hypothesis. We demonstrated a correlation among exon usage, alternative splicing patterns (Fig. 3) and severity of phenotypes in the somites (Fig. 2A,B). Consistent with this finding, a recent study showed a strong correlation between ‘percentage spliced in’ of nonsense mutation-containing exons and DCM severity (Roberts et al., 2015), and another study using engineered induced pluripotent stem cells suggested that nonsense mutations in exons of *TTN* with higher levels of percentage spliced in can cause significant contractile deficits via haploinsufficiency of full-length TTN (Hinson et al., 2015). Our generation of a near-null *ttn* mutant allele by targeting highly used exons in *ttn.2* and *ttn.1* gives more supporting evidence that exon usage is the underlying mechanism (Fig. 5).

A near-null *ttn* mutant validates template functions of titin in assembly of sarcomeres and thick filaments

Generation of the first near-null *ttn* mutant in a vertebrate enables us to genetically test the function of Ttn, which was proposed 20 years ago (Whiting et al., 1989; Trinick, 1996). We found that depletion of Ttn did not affect the alignment of Z-bodies to form a striated pattern at the 12th to 15th somites in an 18-somite embryo (Fig. 6A, C), which indicates that Ttn is not required for assembly of the premyofibrils. Ttn is needed, however, for the formation of nascent myofibrils from premyofibrils, which is characterized as length expansion of the sarcomere from 0.8 to 2.2 μm and widening of the Z-bodies to form Z-disks.

The *ttn^{xu071}* mutant also uncovered two functions of Ttn in thick filament assembly. First, Ttn facilitates the incorporation of the random myosin dots into thin filament networks. When Ttn is absent, myosin filaments remain scattered in the 12th and 15th somites in an 18-somite embryo. Incorporation of the thick filaments into the thin filament networks is delayed until a later developmental stage, as represented by the 6th somite in an 18-somite embryo. Second, Ttn is required for the expansion of the

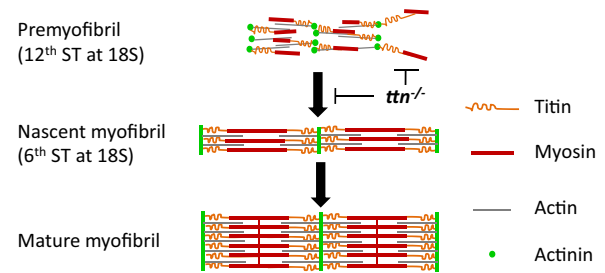


Fig. 9. Schematic indicating functions of titin in *de novo* sarcomere assembly. ST, somite; 18S, 18 somite stage.

rod-like thick filaments, with a length of $\sim 0.8 \mu\text{m}$, to a uniform A-band with a length of $1.6 \mu\text{m}$. This assembly step of the thick filaments is part of the sarcomere assembly step when premyofibrils transform into nascent myofibrils.

Together, our genetic evidence supports the following hypothesis regarding functions of Ttn (Fig. 9). At the premyofibril stage, the Ttn N-terminus binds to the Z-bodies in the existing myofibril network, and its flexible C-terminus binds the thick filaments that are assembled independently and still scattered in the cell (Hill et al., 1986; Wang et al., 1988; Komiyama et al., 1990). Ttn facilitates the incorporation of the thick filaments into the thin filament networks and then guides the lateral alignment of thick filaments and Z-bodies to form mature nascent myofibrils (Fig. 9). Of note, our studies were carried out at the 18 somite stage to eliminate interference from the fast muscle, as its myofibrillogenesis occurs several hours later. Whether our conclusion based on studies in slow muscle is applicable to fast muscle requires future experimental validation. Moreover, our genetic data cannot be used to support the idea that titin functions as a ‘molecular ruler’ to define the length of the A-band – a hypothesis that has also been disproved by a study of a mouse mutant harboring an internal deletion of titin at its I-band/A-band junction (Granzier et al., 2014).

Our data seem to contradict a previous publication stating that the A-band rod domain of Ttn.2 is not essential for thick filament assembly (Myhre et al., 2014). The conclusion was based on *herzschlag*, a *ttn.2* mutant harboring an unidentified mutation mapped to the I-band region of *ttn.2*. It was assumed that the unidentified mutation produced a truncated Ttn.2 protein that loses its thick-filament binding domains, which might not be correct. It is possible that *herzschlag* is a hypomorphic allele but not a null allele.

Implications for TTN-based human diseases

In summary, our studies of a panel of *ttn* mutants uncover functions of Ttn in both *de novo* sarcomere assembly and sarcomere integrity after assembly. Importantly, our data show that a TTNtv cannot be assumed to be a truncating mutation without supporting evidence from a protein gel. Thus, the nomenclature for these nonsense variants as TTNts can be misleading. A slight decrease in the Ttn pool is likely to be sufficient to result in a wide spectrum of phenotypes. The weakened myofibrils have much higher susceptibility to damage incurred by stresses such as muscle contraction.

Caution must be taken when extrapolating these mechanisms uncovered in sarcomere assembly during somitogenesis to cardiomyopathy and muscular dystrophy, which mainly occur in adults. An obvious future direction that is enabled by our study is to raise this panel of *ttn* mutants to adulthood and then assess phenotypes in both heart and muscle. With the convenience of introducing mutations precisely into any exon of *ttn*, it is anticipated

that future studies using the zebrafish model will considerably facilitate our understanding of titinopathy and its related therapies.

MATERIALS AND METHODS

Fish management

Zebrafish were handled following the guidelines of the Mayo Clinic Institutional Animal Care and Use Committee (IACUC protocol A17814). The *WIK* line was used.

Generation of *ttm* mutants via TALENs

TALEN pairs in *ttm.2* and *ttm.1* (Seeley et al., 2007) were designed using Zifit (<http://zifit.partners.org/ZiFiT/ChoiceMenu.aspx>) and assembled using a Golden Gate kit (Addgene) (Cermak et al., 2011). Capped mRNAs were synthesized using mMESAGE mMachine T3 (Ambion) and injected into 1-cell-stage embryos. Successful mutagenesis was confirmed by PCR followed by digestion with restriction enzymes (Table S2). Two mutant alleles that result in two different shifts of reading frame for each mutant locus were selected. Because *ttm.2* and *ttm.1* are located on the same chromosome, double *ttm* mutants were generated by injecting a second TALEN pair into an existing *ttm* mutant.

Vertical agarose gel electrophoresis

Protein samples from zebrafish larvae were extracted by homogenization using a mortar and pestle (Thermo Fisher Scientific) in sample buffer [8 M urea, 3% v/v SDS, 2 M thiourea, 0.05 M Tris-HCl (pH 8.0), 0.03% w/v Bromophenol Blue, 75 mM DTT and 0.01% protease inhibitors (Roche)]. After the samples were incubated in 65°C prewarmed water for 10 min and centrifuged at 4°C for 5 min, the samples were separated on a 2% SDS/agarose gel (30% v/v glycerol, 0.05 M Tris base, 0.384 M glycine, 0.1% w/v SDS and 2% w/v SeaKem Gold agarose) using a vertical agarose gel electrophoresis system (Warren et al., 2003); 1 kb Plus DNA Ladder (Invitrogen) was used for size markers. The gel was fixed in prefixing solution (50% v/v methanol, 12% v/v glacial acetic acid and 5% w/v glycerol), dried in an oven at 50°C overnight and visualized by silver staining (Bio-Rad).

Relative and absolute qPCR studies

Total RNA from 2 dpf zebrafish larvae was extracted using TRIzol (Sigma). Purified RNA (500 ng) was used to generate cDNA using the Superscript III First-Strand Synthesis System (Invitrogen). Relative qPCR was carried out in 96-well QPCR plates (Roche) using a Roche LightCycler 480 QPCR apparatus with the primers listed in Table S2. Gene expression was normalized to the expression level of *glyceraldehyde-3-phosphate dehydrogenase (gapdh)* using $-\Delta\Delta Ct$ (cycle threshold) values. The efficiency of the primers and absolute qPCR was performed using an external standard curve with calibrated 10-fold serial dilutions of the RT-PCR product. Each measurement contained at least three biological replicates and data were analyzed with JMP statistical software.

Whole-mount immunostaining

Dechorionated embryos at the desired stages were fixed in 4% paraformaldehyde in PBS for 20 min at room temperature, permeabilized with 0.1% Triton X-100 in PBS (PBST), blocked in 10% normal sheep serum (Jackson ImmunoResearch) in PBS for 1 h, and stained with primary antibody for 1 h at room temperature. After the embryos were washed in PBST three times for 10 min each, they were incubated for 1 h with secondary antibodies conjugated with Alexa Fluor 488 or 568 (1:1000; Invitrogen). After the embryos were washed in PBST for 10 min three times, they were incubated with the mounting medium with DAPI (Vector Laboratories). Antibodies against the following targets were used: α -Actinin (1:1000; Sigma, A7811), Myosin heavy chain (F59 and A4.1025, both at 1:10; DSHB), Myomesin B4 (mMAC, 1:10; DSHB), Tropomyosin (CH1, 1:200; Sigma, T9283) and Ttn (MIR, 1:200; a gift from the Siegfried Labeit laboratory). Actin filaments were visualized using Alexa Fluor 568 Phalloidin (1:40, Thermo Fisher Scientific). After image acquisition, the genotypes of all embryos used were determined by PCR and restriction enzyme digestion. For each experiment, more than ten mutant embryos were analyzed to confirm the phenotypes.

Microscope image acquisition

After immunostaining, embryos were imaged using a Zeiss Axioplan 2 microscope with Apotome (Zeiss) and an AxioCam Camera (Carl Zeiss) using 20 \times (Plan-Apochromat) and 63 \times (Plan-Neofluar) objective lenses combined with a 10 \times ocular lens. The images were taken and analyzed using AxioVision SE64 4.8.1 software (Zeiss).

Transmission electron microscopy

Embryos at 2 dpf were fixed in Trump's solution (4% paraformaldehyde and 1% glutaraldehyde in 0.1 M phosphate buffer, pH 7.2) at room temperature for 1 h and then overnight at 4°C. Fixed tissues were then embedded in 2% agarose and subsequently processed and imaged at the Mayo Clinic Electron Microscopy Core Facility using a Philips CM10 transmission electron microscope.

Tricaine and blebbistatin treatment

To stop the movement of embryonic somites, embryos at 24 hpf were incubated in E3 water containing either 1% tricaine (Argent Labs) or 10 μ M blebbistatin (Sigma) for 24 h (Yang and Xu, 2012; Yang et al., 2014a). To activate muscle contraction, embryos at 24 dpf were incubated in 0.07% bleach to harden the chorion (Zhang et al., 2009) or treated with 0.5 mM galanthamine (Otten and Abdelilah-Seyfried, 2013).

Statistical analysis

Data were analyzed by JMP software using one-way ANOVA to compare groups. $P < 0.05$ was considered significant. * $P < 0.05$, *** $P < 0.01$ and **** $P < 0.00001$. Data are presented as the mean \pm s.d.

Acknowledgements

We thank Beninio Gore and Kashia Stragey for zebrafish maintenance.

Competing interests

The authors declare no competing or financial interests.

Author contributions

Y.-H.S., A.V.D., P.Z., X.M., M.K. and Y.D.: Acquisition, analysis and interpretation of data; Y.-H.S. and X.X.: Conception and design of the study and drafting or revising the article. All authors approved the manuscript.

Funding

This work was supported by funds from the National Heart, Lung, and Blood Institute (HL81753 and HL107304 to X.X.) and the Mayo Foundation for Medical Education and Research to X.X. Deposited in PMC for release after 12 months.

Supplementary information

Supplementary information available online at <http://dev.biologists.org/lookup/doi/10.1242/dev.139246.supplemental>

References

- Campbell, J. M., Hartjes, K. A., Nelson, T. J., Xu, X. and Ekker, S. C. (2013). New and TALEnted genome engineering toolbox. *Circ. Res.* **113**, 571–587.
- Cermak, T., Doyle, E. L., Christian, M., Wang, L., Zhang, Y., Schmidt, C., Baller, J. A., Somia, N. V., Bogdanove, A. J. and Voytas, D. F. (2011). Efficient design and assembly of custom TALEN and other TAL effector-based constructs for DNA targeting. *Nucleic Acids Res.* **39**, e82.
- Chauveau, C., Rowell, J. and Ferreira, A. (2014). A rising titan: TTN review and mutation update. *Hum. Mutat.* **35**, 1046–1059.
- Devoto, S. H., Melançon, E., Eisen, J. S. and Westerfield, M. (1996). Identification of separate slow and fast muscle precursor cells in vivo, prior to somite formation. *Development* **122**, 3371–3380.
- Gerull, B., Gramlich, M., Atherton, J., McNabb, M., Trombitás, K., Sasse-Klaassen, S., Seidman, J. G., Seidman, C., Granzier, H., Labeit, S. et al. (2002). Mutations of TTN, encoding the giant muscle filament titin, cause familial dilated cardiomyopathy. *Nat. Genet.* **30**, 201–204.
- Gerull, B., Atherton, J., Geupel, A., Sasse-Klaassen, S., Heuser, A., Frenneaux, M., McNabb, M., Granzier, H., Labeit, S. and Thierfelder, L. (2006). Identification of a novel frameshift mutation in the giant muscle filament titin in a large Australian family with dilated cardiomyopathy. *J. Mol. Med.* **84**, 478–483.
- Gramlich, M., Michely, B., Krohne, C., Heuser, A., Erdmann, B., Klaassen, S., Hudson, B., Magarin, M., Kirchner, F., Todiras, M. et al. (2009). Stress-induced dilated cardiomyopathy in a knock-in mouse model mimicking human titin-based disease. *J. Mol. Cell. Cardiol.* **47**, 352–358.

- Granzier, H. L. and Labeit, S.** (2004). The giant protein titin: a major player in myocardial mechanics, signaling, and disease. *Circ. Res.* **94**, 284-295.
- Granzier, H. L., Hutchinson, K. R., Tonino, P., Methawasin, M., Li, F. W., Slater, R. E., Bull, M. M., Saripalli, C., Pappas, C. T., Gregorio, C. C.** et al. (2014). Deleting titin's I-band/A-band junction reveals critical roles for titin in biomechanical sensing and cardiac function. *Proc. Natl. Acad. Sci. USA* **111**, 14589-14594.
- Guo, W., Bharmal, S. J., Esbona, K. and Greaser, M. L.** (2010). Titin diversity—alternative splicing gone wild. *J. Biomed. Biotechnol.* **2010**, 753675.
- Hackman, P., Vihola, A., Haravuori, H., Marchand, S., Sarparanta, J., de Seze, J., Labeit, S., Witt, C., Peltonen, L., Richard, I.** et al. (2002). Tibial muscular dystrophy is a titinopathy caused by mutations in TTN, the gene encoding the giant skeletal-muscle protein titin. *Am. J. Hum. Genet.* **71**, 492-500.
- Herman, D. S., Lam, L., Taylor, M. R. G., Wang, L., Teekakirikul, P., Christodoulou, D., Conner, L., DePalma, S. R., McDonough, B., Sparks, E.** et al. (2012). Truncations of titin causing dilated cardiomyopathy. *N. Engl. J. Med.* **366**, 619-628.
- Hill, C. S., Duran, S., Lin, Z. X., Weber, K. and Holtzer, H.** (1986). Titin and myosin, but not desmin, are linked during myofibrillogenesis in postmitotic mononucleated myoblasts. *J. Cell Biol.* **103**, 2185-2196.
- Hinson, J. T., Chopra, A., Nafissi, N., Polacheck, W. J., Benson, C. C., Swist, S., Gorham, J., Yang, L., Schafer, S., Sheng, C. C.** et al. (2015). HEART DISEASE. Titin mutations in iPSC cells define sarcomere insufficiency as a cause of dilated cardiomyopathy. *Science* **349**, 982-986.
- Huang, W., Zhang, R. and Xu, X.** (2009). Myofibrillogenesis in the developing zebrafish heart: A functional study of *tnnt2*. *Dev. Biol.* **331**, 237-249.
- Kok, F. O., Shin, M., Ni, C.-W., Gupta, A., Grosse, A. S., van Impel, A., Kirchmaier, B. C., Peterson-Maduro, J., Kourkoulis, G., Male, I.** et al. (2015). Reverse genetic screening reveals poor correlation between morpholino-induced and mutant phenotypes in zebrafish. *Dev. Cell* **32**, 97-108.
- Komiyama, M., Maruyama, K. and Shimada, Y.** (1990). Assembly of connectin (titin) in relation to myosin and alpha-actinin in cultured cardiac myocytes. *J. Muscle Res. Cell Motil.* **11**, 419-428.
- Labeit, S. and Kolmerer, B.** (1995). Titins: giant proteins in charge of muscle ultrastructure and elasticity. *Science* **270**, 293-296.
- Labeit, S., Gautel, M., Lakey, A. and Trinick, J.** (1992). Towards a molecular understanding of titin. *EMBO J.* **11**, 1711-1716.
- LeWinter, M. M. and Granzier, H. L.** (2013). Titin is a major human disease gene. *Circulation* **127**, 938-944.
- McKeown, K. A., Downes, G. B. and Hutson, L. D.** (2009). Modular laboratory exercises to analyze the development of zebrafish motor behavior. *Zebrafish* **6**, 179-185.
- Myhre, J. L., Hills, J. A., Prill, K., Wohlgemuth, S. L. and Pilgrim, D. B.** (2014). The titin A-band rod domain is dispensable for initial thick filament assembly in zebrafish. *Dev. Biol.* **387**, 93-108.
- Norton, N., Li, D., Rampersaud, E., Morales, A., Martin, E. R., Zuchner, S., Guo, S., Gonzalez, M., Hedges, D. J., Robertson, P. D.** et al. (2013). Exome sequencing and genome-wide linkage analysis in 17 families illustrate the complex contribution of TTN truncating variants to dilated cardiomyopathy. *Circ. Cardiovasc. Genet.* **6**, 144-153.
- Otten, C. and Abdelilah-Seyfried, S.** (2013). Laser-inflicted injury of zebrafish embryonic skeletal muscle. *J. Vis. Exp.* **17**, e4351.
- Radke, M. H., Peng, J., Wu, Y., McNabb, M., Nelson, O. L., Granzier, H. and Gotthardt, M.** (2007). Targeted deletion of titin N2B region leads to diastolic dysfunction and cardiac atrophy. *Proc. Natl. Acad. Sci. USA* **104**, 3444-3449.
- Roberts, A. M., Ware, J. S., Herman, D. S., Schafer, S., Baksi, J., Bick, A. G., Buchan, R. J., Walsh, R., John, S., Wilkinson, S.** et al. (2015). Integrated allelic, transcriptional, and phenomic dissection of the cardiac effects of titin truncations in health and disease. *Sci. Transl. Med.* **7**, 270ra6.
- Rossi, A., Kontarakis, Z., Gerri, C., Nolte, H., Hölper, S., Krüger, M. and Stainier, D. Y. R.** (2015). Genetic compensation induced by deleterious mutations but not gene knockdowns. *Nature* **524**, 230-233.
- Sanger, J. W., Wang, J., Holloway, B., Du, A. and Sanger, J. M.** (2009). Myofibrillogenesis in skeletal muscle cells in zebrafish. *Cell Motil. Cytoskelet.* **66**, 556-566.
- Schoenebeck, J. J. and Yelon, D.** (2007). Illuminating cardiac development: advances in imaging add new dimensions to the utility of zebrafish genetics. *Semin. Cell Dev. Biol.* **18**, 27-35.
- Seeley, M., Huang, W., Chen, Z., Wolff, W. O., Lin, X. and Xu, X.** (2007). Depletion of zebrafish titin reduces cardiac contractility by disrupting the assembly of Z-discs and A-bands. *Circ. Res.* **100**, 238-245.
- Steffen, L. S., Guyon, J. R., Vogel, E. D., Howell, M. H., Zhou, Y., Weber, G. J., Zon, L. I. and Kunkel, L. M.** (2007). The zebrafish *runzel* muscular dystrophy is linked to the titin gene. *Dev. Biol.* **309**, 180-192.
- Straight, A. F., Cheung, A., Limouze, J., Chen, I., Westwood, N. J., Sellers, J. R. and Mitchison, T. J.** (2003). Dissecting temporal and spatial control of cytokinesis with a myosin II Inhibitor. *Science* **299**, 1743-1747.
- Trinick, J.** (1996). Cytoskeleton: titin as a scaffold and spring. *Curr. Biol.* **6**, 258-260.
- Udd, B., Vihola, A., Sarparanta, J., Richard, I. and Hackman, P.** (2005). Titinopathies and extension of the M-line mutation phenotype beyond distal myopathy and LGMD2J. *Neurology* **64**, 636-642.
- Wang, S. M., Greaser, M. L., Schultz, E., Bulinski, J. C., Lin, J. J. and Lessard, J. L.** (1988). Studies on cardiac myofibrillogenesis with antibodies to titin, actin, tropomyosin, and myosin. *J. Cell Biol.* **107**, 1075-1083.
- Warren, C. M., Krzesinski, P. R. and Greaser, M. L.** (2003). Vertical agarose gel electrophoresis and electroblotting of high-molecular-weight proteins. *Electrophoresis* **24**, 1695-1702.
- Weinert, S., Bergmann, N., Luo, X., Erdmann, B. and Gotthardt, M.** (2006). M line-deficient titin causes cardiac lethality through impaired maturation of the sarcomere. *J. Cell Biol.* **173**, 559-570.
- Whiting, A., Wardale, J. and Trinick, J.** (1989). Does titin regulate the length of muscle thick filaments? *J. Mol. Biol.* **205**, 263-268.
- Xu, X., Meiler, S. E., Zhong, T. P., Mohideen, M., Crossley, D. A., Burggren, W. W. and Fishman, M. C.** (2002). Cardiomyopathy in zebrafish due to mutation in an alternatively spliced exon of titin. *Nat. Genet.* **30**, 205-209.
- Yang, J. and Xu, X.** (2012). alpha-Actinin2 is required for the lateral alignment of Z discs and ventricular chamber enlargement during zebrafish cardiogenesis. *FASEB J.* **26**, 4230-4242.
- Yang, J., Hartjes, K. A., Nelson, T. J. and Xu, X.** (2014a). Cessation of contraction induces cardiomyocyte remodeling during zebrafish cardiogenesis. *Am. J. Physiol. Heart Circ. Physiol.* **306**, H382-H395.
- Yang, J., Shih, Y.-H. and Xu, X.** (2014b). Understanding cardiac sarcomere assembly with zebrafish genetics. *Anat. Rec.* **297**, 1681-1693.
- Zhang, R., Yang, J., Zhu, J. and Xu, X.** (2009). Depletion of zebrafish Tcap leads to muscular dystrophy via disrupting sarcomere-membrane interaction, not sarcomere assembly. *Hum. Mol. Genet.* **18**, 4130-4140.
- Zou, J., Tran, D., Baalbaki, M., Tang, L. F., Poon, A., Pelonero, A., Titus, E. W., Yuan, C., Shi, C., Patchava, S.** et al. (2015). An internal promoter underlies the difference in disease severity between N- and C-terminal truncation mutations of Titin in zebrafish. *Elife* **4**, e09406.

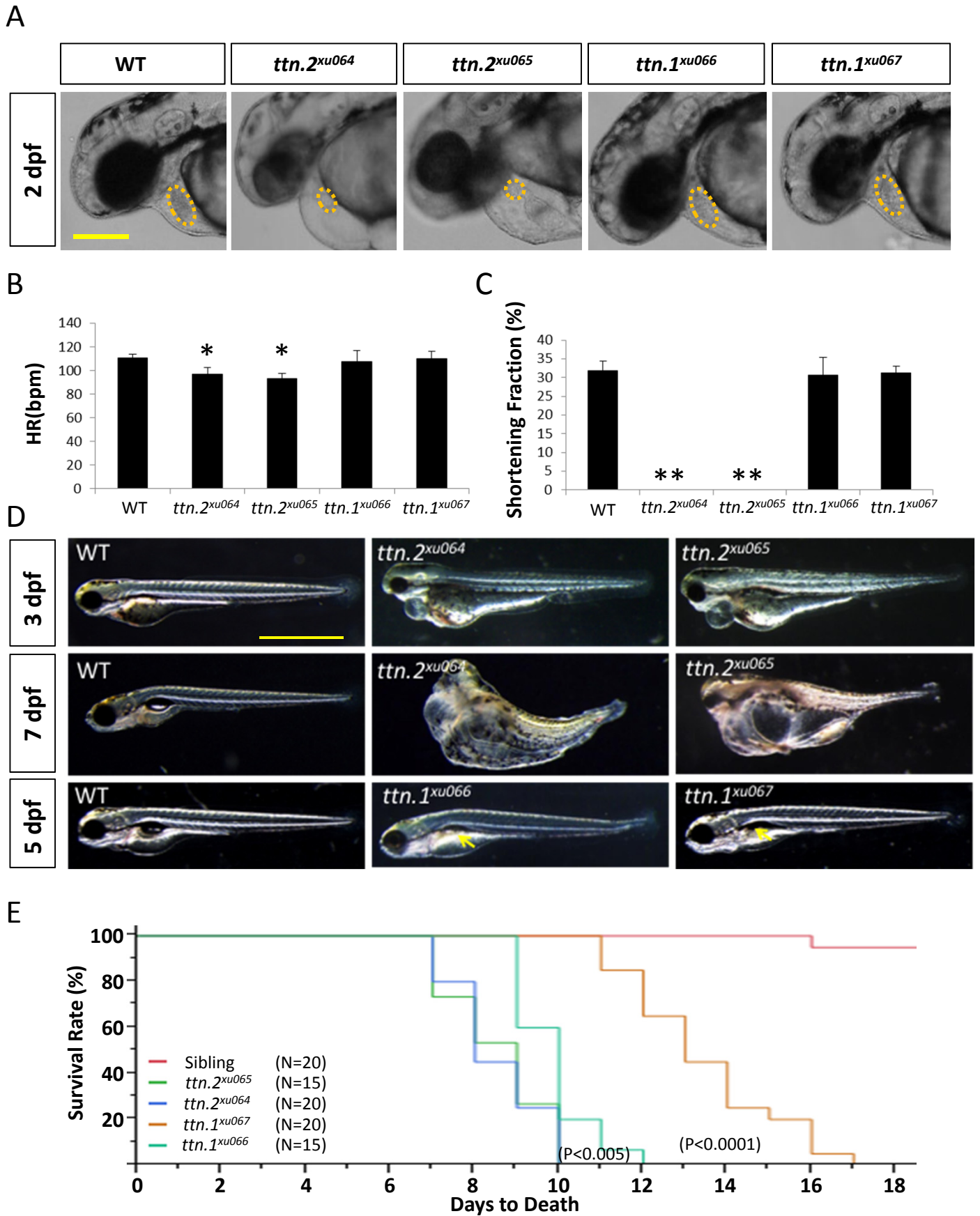


Figure S1.

Figure S1. Phenotypes of *ttn.2* and *ttn.1* mutants. A, Cardiac edema with decreased ventricle size (dashed circles) was noted in both *ttn.2^{xu064}* and *ttn.2^{xu065}*, but not in *ttn.1^{xu066}* and *ttn.1^{xu067}*. Shown are bright-field images at 2 dpf. Scale bar, 0.05 mm. B and C, In *ttn.2^{xu064}* and *ttn.2^{xu065}*, the heart rate was slightly decreased (B), and the ventricular shortening fraction was reduced to zero (C). * and ** indicates $p < 0.05$ and $p < 0.01$, respectively. Means \pm S.D. N=5. D, Bright-field images demonstrated that the cardiac edema was still present in both *ttn.2^{xu064}* and *ttn.2^{xu065}* at 3 dpf, but muscle disarray was more obvious in *ttn.2^{xu065}*. Both *ttn.2* mutants had whole-body edema at 7 dpf. *ttn.1^{xu066}* and *ttn.1^{xu067}* showed deflation of the swim bladder at 5 dpf (arrows). Scale bar, 1 mm. E, *ttn.2^{xu064}* and *ttn.2^{xu065}* mutants started to die at 7 dpf and could survive up to 10 dpf; *ttn.1^{xu066}* could survive until 12 dpf; and *ttn.1^{xu067}* started to die at 11 dpf and could live up to 17 dpf.

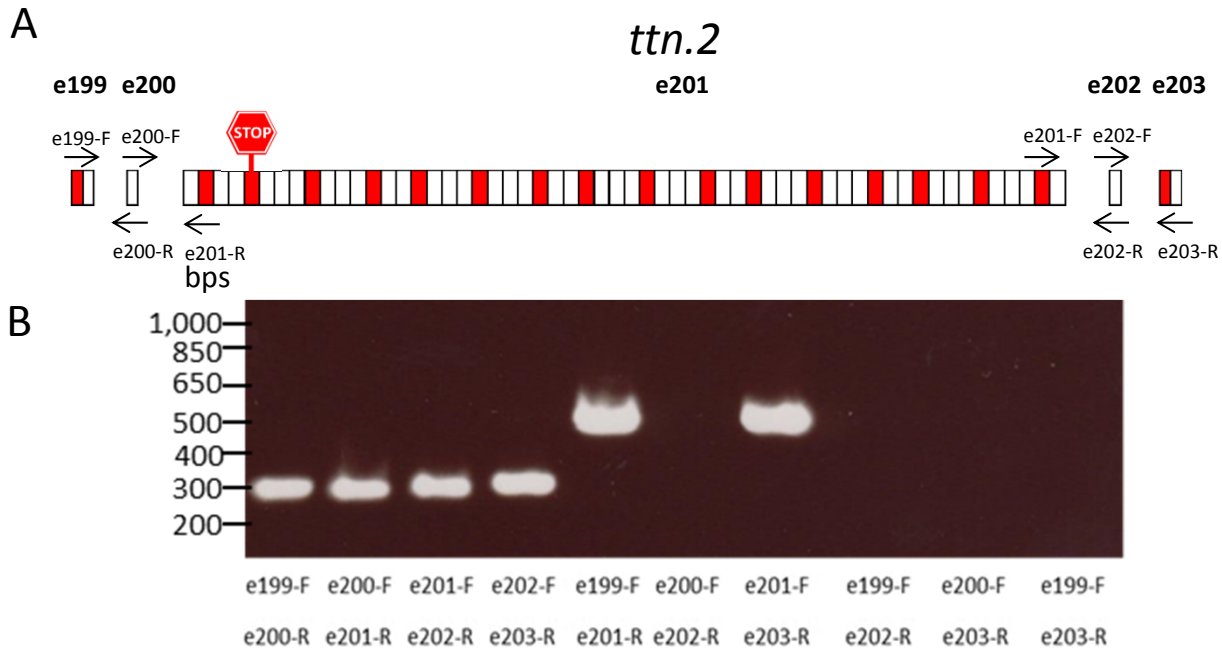
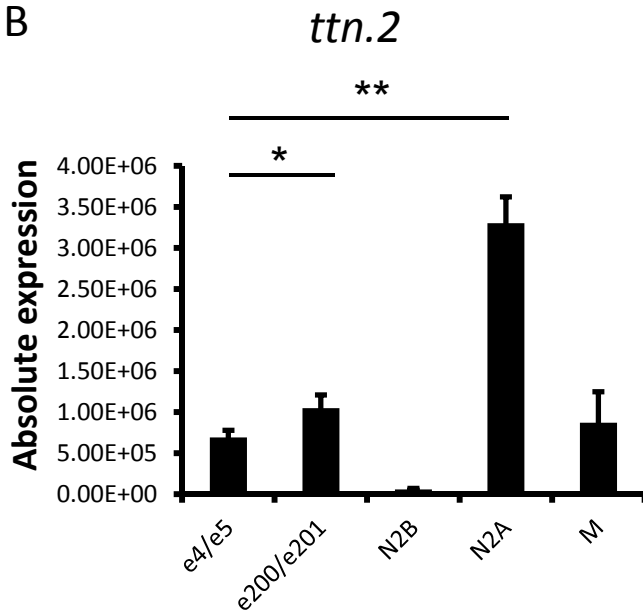


Figure S2. No Exon Skipping of Exon 201 of *ttn.2*. A, RT-PCR using different combinations of forward and reverse primers targeted to exons around 199-203 of *ttn.2*. B, RT-PCR using different combinations of primers showed no exon-skipping event.

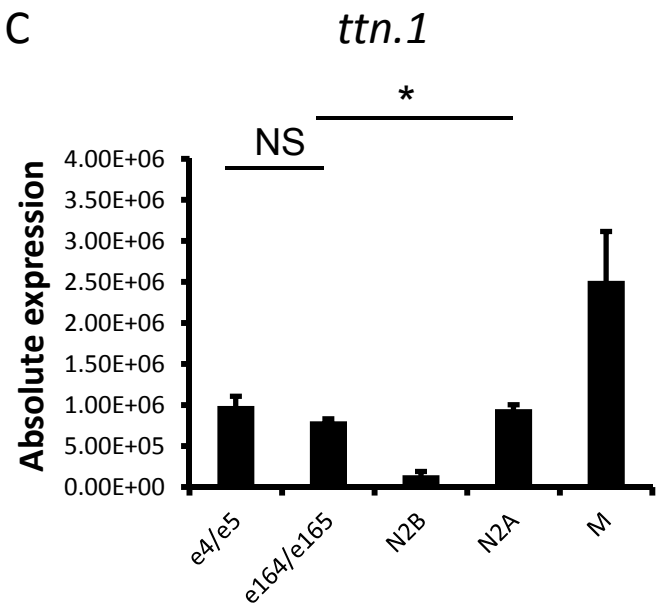
A

<i>ttn.2</i>		<i>ttn.1</i>	
e4/e5	98.9%	e4/e5	91.8%
e200/e201	93.4%	e164/e165	94.9%
N2B	98.1%	N2B	98%
N2A	98.1%	N2A	98.8%
M	91.7%	M	95.2%

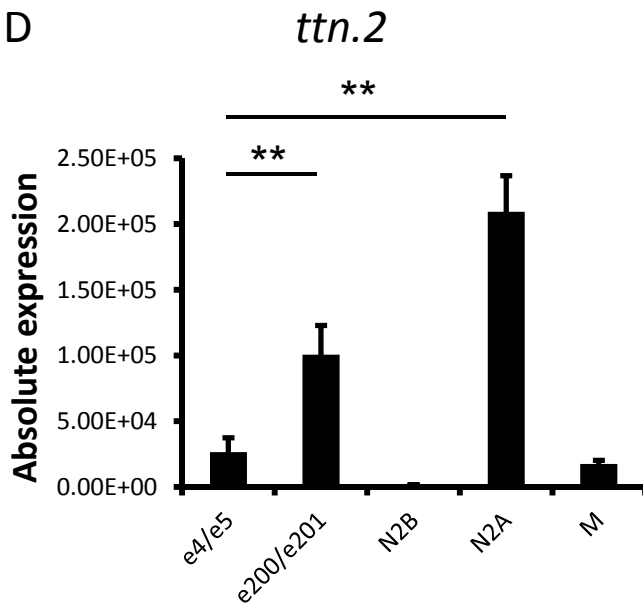
B



C



D



E

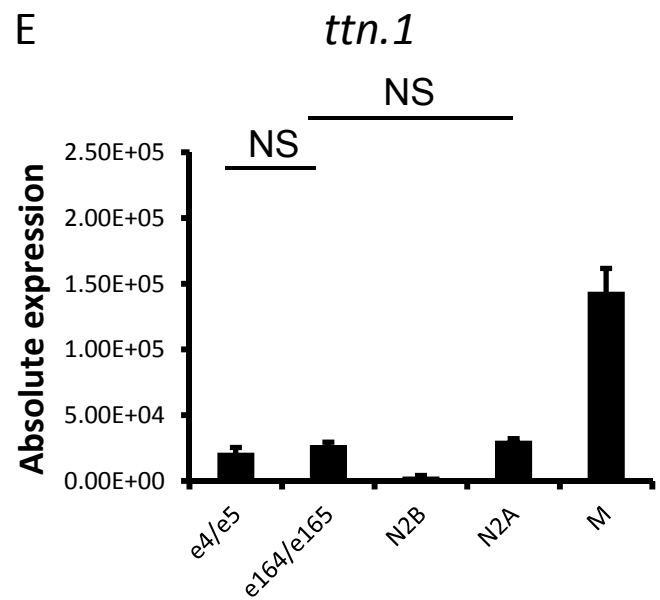


Figure S3.

Figure S3. Usage of Different Exons in *ttn.2* and *ttn.1* in 5 dpf and 9 dpf WT embryos. A, Efficiency of the primers in *ttn.2* and *ttn.1* was obtained by qPCR using standard curve. B and C, Exon usage was quantified using absolute qPCR with primers targeting exons in *ttn.2* (B) and *ttn.1* (C) in 5 dpf WT embryos. Means \pm S.D. N=9. D and E, Usage of exons of *ttn.2* (D) and *ttn.1* (E) in 9 dpf WT embryos. Means \pm S.D. N=9. * indicates $p < 0.05$, ** indicates $p < 0.01$, NS indicates not statistically significant ($p > 0.05$).

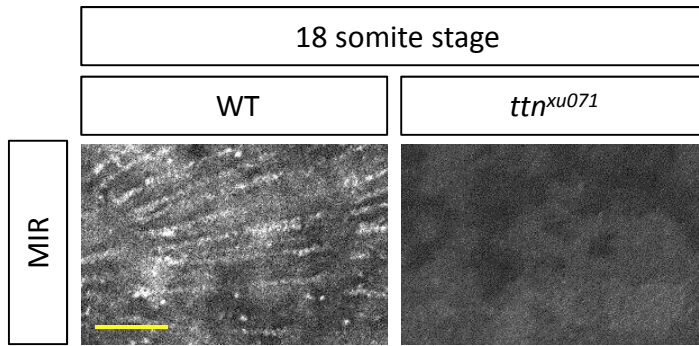


Figure S4. The Assembly of Titin Into Premyofibrils. Titin isoforms were assembled into premyofibrils and became striated at the 12th somite of an 18-somite embryo, as indicated by immunostaining using MIR, an anti-Titin antibody. Loss of Titin in somites in the *ttn^{xu071}* mutant has been seen. Scale bar, 20 μm .

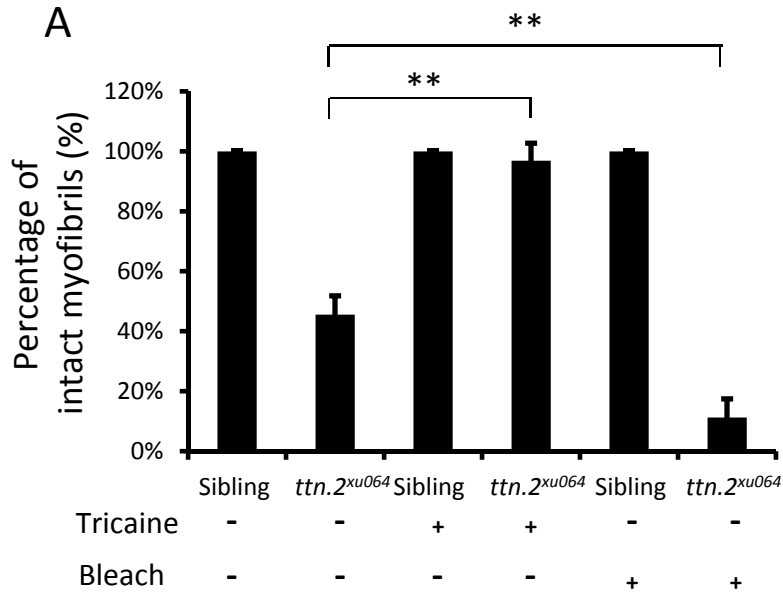


Figure S5. Inhibiting or inducing muscle contraction exert opposite effects on myofibril damage in the slow muscle of *ttn.2^{xu064}*. Shown are percentage of intact myofibrils out of total myofibrils at the 8th to 12th somites of larvae. Representative images are shown in Fig. 8C. Means \pm S.D. N=5. ** indicates $p < 0.01$. Tricaine treatment significantly prevented the breakage of myofibrils in *ttn.2^{xu064}*. Conversely, bleach treatment significantly increased the breakage of myofibrils in *ttn.2^{xu064}*. Siblings include both WT and heterozygotes.

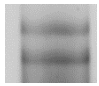
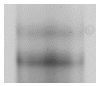
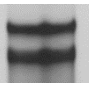
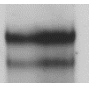
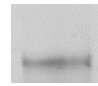
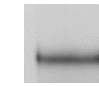

Mutants	<i>ttn.1^{xu067}</i>	<i>ttn.1^{xu066}</i>	<i>ttn.2^{xu064}</i>	<i>ttn.2^{xu065}</i>	<i>ttn^{xu069}</i>	<i>ttn^{xu070}</i>	<i>ttn^{xu071}</i>
Ttn Expression							
Phenotypes in somites	N.A.	9 dpf	2 dpf (S)	18S (m)	18S	18S	18S
	Sarcomere stability			<i>de novo</i> Sarcomere assembly			

Figure S6. Summary of Ttn protein expression and sarcomeric phenotypes in 7 *ttn* mutants. (S) indicates slow muscle-specific phenotypes; 18S, 18-somite stage; N.A., not available; (m), mild phenotypes, as represented by occasional striated structures (See inset in Fig. 2A).

Table S1. Nomenclature of *ttn* mutants

[Click here to Download Table S1](#)

Table S2. Primers list for genotyping (A) and polymerase chain reaction (B).**A.**

allele	Forward Primer	Reverse Primer	Restriction Enzyme	Size of PCR product	Size of PCR product after digestion
<i>xu64</i> , <i>xu68</i> , <i>xu69</i>	TGCATTTTCATTGGTTCACAG	CCTCACAGGAGAGGGAGACT	EcoRV	406	81, 325
<i>xu65</i> , <i>xu68</i> , <i>xu70</i> , <i>xu71</i>	ACAAACTGGCAGAAATGCTC	GTCGACTTTCTCGAGTTCA	HindIII	403	304, 99
<i>xu66</i> , <i>xu69</i> , <i>xu71</i>	TGGTTTCACCCAAATTTAC	CTTTAACAGGCCTCACAGGA	CaC8I	453	120, 333
<i>xu67</i> , <i>xu70</i>	TGGGAAATGCCTCTTATTGA	GATGACTTCGCCAGAATA	BglII	480	131, 349

B.

	Primer	Note		Primer	Note
ttn.2-e4-F	CCGCTGACTTTCAGATTGTT	†	ttn.1-M-R	GGACTGCACTTCTCATAGGT	§ †
ttn.2-e5-R	CGAGTCTGACGAGTTTGTGA	†	gapdh-F	CCACCCATGGAAAGTACAAG	§ #
ttn.2-e200-F	GTTTTGGTGAACCCAGTGAG	† ^	gapdh-R	CTCTCTTTGCACCACCCTTA	§ #
ttn.2-e201-R	AAGCGCACTGACTCTGAAGT	† ^	ttn.2-e2-F	CAGGCACCAACATTTACACA	%
ttn.2-N2B-F	CACAAACCGTTGTACTTTCA	†	ttn.2-e7-R	GGAGGTCTGGACTTGTGTTG	%
ttn.2-N2B-R	TTCTCTTAGGGGTTGCACTG	†	ttn.1-e2-F	AACATTTACACAGCCGCTTC	%
ttn.2-N2A-F	TGCAGCACTGACTTGAATGT	†	ttn.1-e7-R	AACATAACCCTCTGCTTCC	%
ttn.2-N2A-R	TCGATAGCTTGAAGGAGACC	†	ttn.2-e199-F	GTCTGGACCAGTCAAATGG	^
ttn.2-M-F	CTCTTTTGTGGGCAAGTGT	§ †	ttn.2-e200-R	CTCACTGGGTTCAACAAAAC	^
ttn.2-M-R	AATGATGCCTCTTGCATTGT	§ †	ttn.2-e201-F	GTGGTGCTCCAGTCAAAAAC	^
ttn.1-e4-F	CCGCTGACTTTCAGATTGTT	†	ttn.2-e202-R	CTTCCTCCATCATGTTCTGG	^
ttn.1-e5-R	CCTGGCGAGTCTGTGAAAT	†	ttn.2-e202-F	CCAGAACATGATGGAGGAAG	^
ttn.1-	GTGAACCCTCAATTCCTGTG	† *	ttn.2-	CCAGTAAGGGGGATCTCAAT	^

e164-F			e203-R		
ttn.1-e165-R	ACTTCAGTCCAGCTTCCAAA	† *	ttn.1-e163-F	CTGGTGATGCCTCTCACTCT	*
ttn.1-N2B-F	GCTACAGTGTACCCGAAGGA	†	ttn.1-e164-R	ATGCTCGTGTCCATCTCATT	*
ttn.1-N2B-R	TGCATTTCAAAGATTTCTCTT	†	ttn.1-e165-F	AGGCCTGGGTATGTGTATCA	*
ttn.1-N2A-F	TTGCTAAAGTCGGTGGTGAT	†	ttn.1-e166-R	TCCACCATCAAACCTCTGGTT	*
ttn.1-N2A-R	GGCCAGACTCTTTCTTCTC	†	ttn.1-e166-F	GACTCAGTGAGCCCAAAGAA	*
ttn.1-M-F	CATGGTTCAGCACATCTTGA	§ †	ttn.1-e167-R	CTAAATCGCTTGCCACACTT	*

§: Primers used in Fig. 1D-E and 4D and 5C

†: Primers used in Fig. 3A-B and Fig. S3

‡: Primers used in Fig. 3C

^: Primers used in Fig. S2

*: Primers used in Fig. 3E-F